PNAS RESEARCH ARTICLE | BIOCHEMISTRY OPEN ACCESS

Isoform-specific C-terminal phosphorylation drives autoinhibition of Casein kinase 1

Rachel L. Harold[a,1], Nikhil K. Tulsian[b,c,1], Rajesh Narasimamurthy[d], Noelle Yaitanes[a], Maria G. Ayala Hernandez[a], Hsiau-Wei Lee[a], Priya Crosby[a], Sarvind M. Tripathi[a], David M. Virshup[d,e,2], and Carrie L. Partch[a,f,g,2]

Affiliations are included on p. 10.

Edited by Brian R. Crane, Cornell University, Ithaca, NY; received August 12, 2024; accepted August 31, 2024 by Editorial Board Member Jay C. Dunlap

Casein kinase 1δ (CK1δ) controls essential biological processes including circadian rhythms and wingless-related integration site (Wnt) signaling, but how its activity is regulated is not well understood. CK1δ is inhibited by autophosphorylation of its intrinsically disordered C-terminal tail. Two CK1 splice variants, δ1 and δ2, are known to have very different effects on circadian rhythms. These variants differ only in the last 16 residues of the tail, referred to as the extreme C termini (XCT), but with marked changes in potential phosphorylation sites. Here, we test whether the XCT of these variants have different effects in autoinhibition of the kinase. Using NMR and hydrogen/deuterium exchange mass spectrometry, we show that the δ1 XCT is preferentially phosphorylated by the kinase and the δ1 tail makes more extensive interactions across the kinase domain. Mutation of δ1-specific XCT phosphorylation sites increases kinase activity both in vitro and in cells and leads to changes in the circadian period, similar to what is reported in vivo. Mechanistically, loss of the phosphorylation sites in XCT disrupts tail interaction with the kinase domain. δ1 autoinhibition relies on conserved anion-binding sites around the CK1 active site, demonstrating a common mode of product inhibition of CK1δ. These findings demonstrate how a phosphorylation cycle controls the activity of this essential kinase.

circadian rhythms | kinase | intrinsically disordered proteins

Significance

Subtle control of kinase activity is critical to physiologic modulation of multiple physiological processes including circadian rhythms. Casein kinase 1δ (CK1δ) and the closely related Casein kinase 1 epsilon (CK1ε) regulate circadian rhythms by phosphorylation of PERIOD2 (PER2), but how kinase activity itself is controlled is not clear. Building on the prior observation that two splice isoforms of CK1δ have opposite effects on the circadian period, we show that the difference maps to three phosphorylation sites specific to δ1 in the variably spliced region [extreme C termini (XCT)] that cause feedback inhibition of the kinase domain. More broadly, the data suggest a general model where CK1 activity on diverse substrates can be controlled by signaling pathways that alter tail phosphorylation.

Kinases play a crucial role in biology through their ability to posttranslationally modify proteins by phosphorylation, altering the structure and/or activity of their targets. The activity of most kinases is therefore kept under tight regulation, requiring phosphorylation of their activation loops and/or binding to cofactors or scaffolds to remodel the active site and recruit substrates. In some cases, removal of inhibitory phosphorylation can activate kinases (1, 2). The kinase domains of Casein kinase 1δ (CK1δ) and its paralog, Casein kinase 1 epsilon (CK1ε), are constitutively active, but autophosphorylation of their intrinsically disordered C-terminal extensions, or "tails," inhibits kinase activity (3, 4). CK1δ/ε tails are also targeted by a number of other kinases (5, 6) and phosphatases (4, 7–9) in vivo, indicating a dynamic mode of kinase regulation that is not well understood. Given the involvement of CK1δ/ε in a wide range of pathways from wingless-related integration site (Wnt) signaling, cell division, and apoptosis to circadian rhythms (5), understanding how the kinase activity of CK1δ/ε is regulated by phosphorylation of their intrinsically disordered tails could shed light on underappreciated regulatory mechanisms.

In mammalian circadian rhythms, CK1δ/ε regulate the intrinsic timing of the molecular clock through phosphorylation of the Period (PER) proteins (10–12). A phosphoswitch involving competing CK1δ/ε-dependent sites on PERIOD2 (PER2) regulates its half-life (13), wherein phosphorylation of beta-transduction repeat containing protein degrons and subsequent protein turnover are counteracted by phosphorylation of several serines located within the CK1 binding domain that anchors the kinase to PER throughout its daily life cycle (14–17). These stabilizing phosphorylation sites occur within the Familial Advanced Sleep Phase (FASP) region, named for a point mutation in human PER2 (S662G) that eliminates the priming phosphorylation and shortens the clock by ~4 h (18, 19). We recently showed that phosphorylation of the PER2 FASP region leads to feedback inhibition of the anchored kinase, utilizing two highly conserved anion-binding sites on CK1δ near the active site that bind phosphoserines in the FASP to block access to substrates (20). This is similar to feedback inhibition of the kinase observed in DNA damage-induced apoptosis (21). Conservation of these feedback inhibition binding modes establishes the importance of CK1δ/ε anion-binding sites for regulation of the kinase by phosphorylated substrates.

Seemingly modest alterations in CK1δ/ε activity are well established to shift the balance of the phosphoswitch to have a profound effect on circadian timing in mammals from

The authors declare no competing interest.

This article is a PNAS Direct Submission. B.R.C. is a guest editor invited by the Editorial Board.

[1]R.L.H. and N.K.T. contributed equally to this work.

[2]To whom correspondence may be addressed. Email: david.virshup@duke.edu or cpartch@ucsc.edu.

This article contains supporting information online at https://www.pnas.org/lookup/suppl/doi:10.1073/pnas.2415567121/-/DCSupplemental.

Published October 2, 2024.

rodents to humans. These alterations include inherited polymorphisms (22–25) and alternative splicing of CK1δ (26). The two CK1δ splice isoforms, δ1 and δ2, are identical throughout the kinase domain and most of the intrinsically disordered tail, differing only in the last 16 amino acids of the C terminus (Fig. 1*A*), a region we call here the extreme C terminus or extreme C termini (XCT). Despite this relatively minor change, the δ1 and δ2 isoforms differentially phosphorylate the PER2 FASP region in vivo to control the circadian period (26). Truncating the XCT at residue 400 is sufficient to derepress kinase activity (27), suggesting a crucial role for the XCT in regulation of CK1 activity in cells.

In this study, to understand how the splice variants differentially regulate clock speed, we examined the biochemical role of the XCT in the regulation of CK1δ isoform activity. We found that isoform-specific differences in CK1 activity are intrinsic to the kinase in vitro; CK1δ1 is autoinhibited to a greater extent than CK1δ2, and truncation of the isoform-specific XCT essentially eliminates autoinhibition. NMR assays of the δ1 tail with the kinase domain in *trans* or *cis*, via segmental isotopic labeling, revealed that the interaction between the kinase domain and δ1 tail is dependent on phosphorylation and predominantly localized to the δ1-specific sequence. By contrast, the δ2 tail interacts with the kinase domain even in the absence of phosphorylation, consistent with inhibition data using isolated δ1 or δ2 peptides. Biochemically, mutation of three phosphosites in the unique region of CK1δ1 increased its activity to that of CK1δ2. Using hydrogen/deuterium exchange mass spectrometry (HDX-MS), we mapped how CK1 isoforms or mutants differentially protect the kinase domain and intrinsically disordered tails from deuterium exchange. Protection of the kinase active site in the presence of an inhibitory phosphoFASP peptide of PER2 (20) mirrors protection by the two CK1δ isoforms, which is largely eliminated

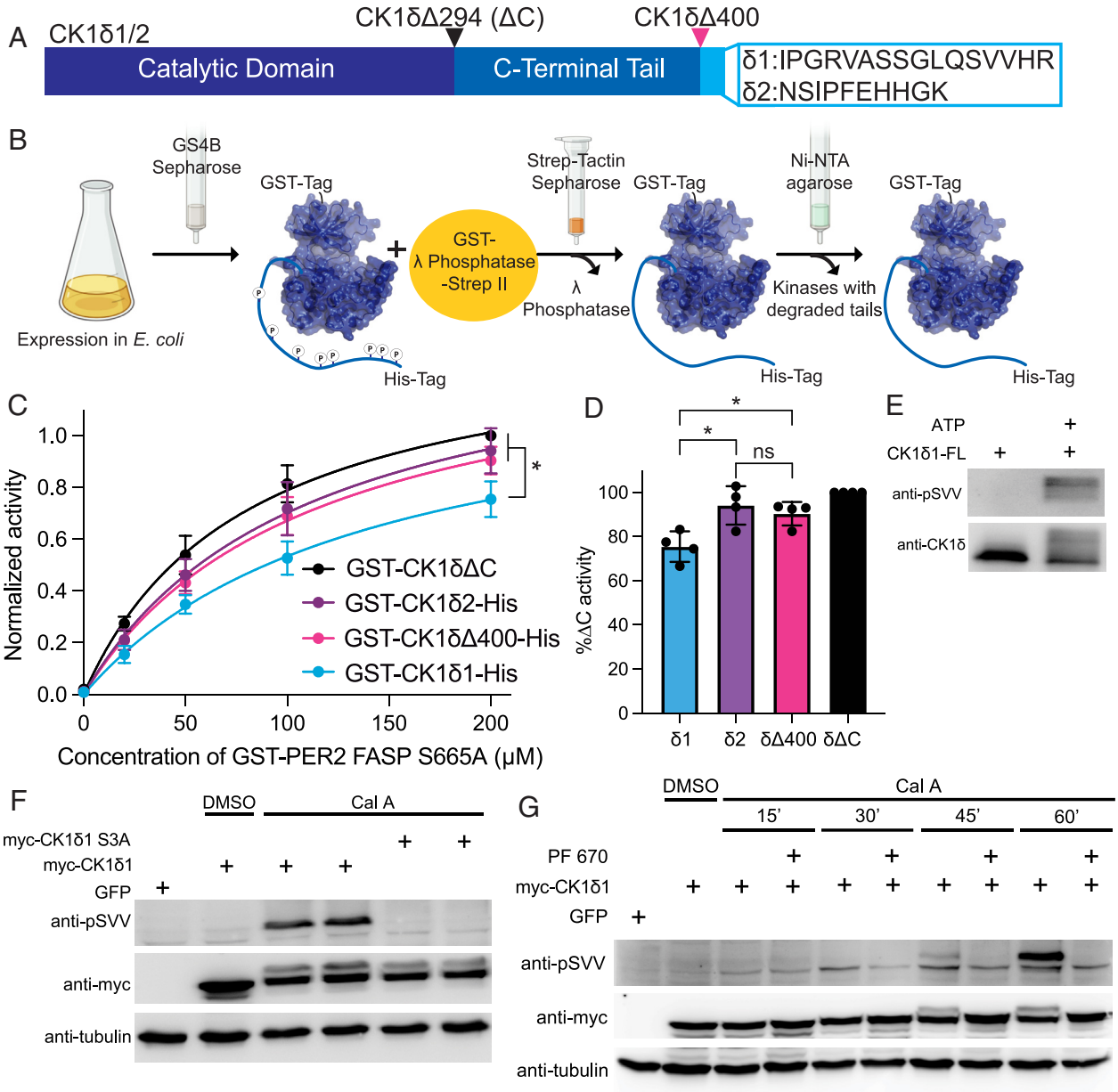

Fig. 1. CK1δ isoforms change kinase activity in vitro and regulation of XCT phosphorylation in cells. (*A*) Schematic of CK1δ isoforms and truncations. (*B*) Kinase purification scheme with double tag system. (*C*) Quantification of ^{32}P kinase assay measuring priming phosphorylation by CK1δ1 (blue), CK1δ2 (purple), CK1δΔ400 (pink), or CK1δΔC (black), normalized to max activity of CK1δΔC. Significance was assessed by the extra sum-of-squares F test (n = 4, mean ± SD). (*D*) Quantification of endpoint (200 μM) in panel *C*. Ordinary one-way ANOVA, *$P < 0.05$ (n = 4, mean ± SD). (*E*) Representative western blot of purified CK1δ1 autophosphorylation detected with phospho-Serine, Valine, Valine (pSVV) ab (n = 3). (*F*) Representative western blot of myc-CK1δ1 or myc-CK1δ1 S3A (S406/S407/S411A) phosphorylation in cells treated with calyculin A (n = 3). (*G*) Representative western blot of CK1δ1 phosphorylation in cells treated with Cal A and PF 670 (n = 3).

by deleting the XCT region with the Δ400 truncation or mutation of the three δ1-specific phosphosites. These biochemical findings translate in cells, where mutation of the δ1-specific phosphosites increases kinase activity and affects the period of the cell's circadian rhythm. Our study defines isoform-specific mechanisms of CK1δ regulation and demonstrates a conserved mechanism of kinase inhibition by phosphorylated substrates.

Results

CK1δ Isoforms δ1 and δ2 Have Different Kinase Activity In Vitro. The alternatively spliced CK1δ isoforms, δ1 and δ2, differ only in the last 16 amino acids of the C-terminal tail (Fig. 1*A*). We previously showed that CK1δ1, CK1δ2, and a related isoform, CK1ε, can all catalyze the rate-limiting priming phosphorylation of PER2 FASP, with CK1δ2 and CK1ε demonstrating increased activity compared to CK1δ1 (27). This is biologically relevant, as CK1δ1 expression causes a shorter circadian period than CK1δ2 (26). The kinase domains of CK1δ and CK1ε are highly conserved, and though their intrinsically disordered C-terminal tails differ, the XCT of CK1δ2 and CK1ε are quite similar but dissimilar to the XCT of CK1δ1 (*SI Appendix*, Fig. S1*A*). This suggested that the differences in biological activity we observed in cells might be due to their XCT; consistent with this, truncation of the XCT of CK1δ1 (Δ400) eliminated its isoform-specific decrease in activity (27).

To determine whether isoform-specific differences in activity are intrinsic to the kinase, we established a pipeline to purify dephosphorylated full-length recombinant proteins (Fig. 1*B*). To demonstrate the effect of tail phosphorylation on CK1δ1, we first pretreated full-length dephosphorylated CK1δ1 with adenosine triphosphate (ATP) to induce autophosphorylation and then measured its activity on the PER2 FASP priming site. As expected, pretreatment of the kinase with ATP before the substrate was added significantly reduced FASP priming phosphorylation compared to untreated CK1δ1 (*SI Appendix*, Fig. S1*B*). We then used in vitro kinase assays to measure the activity of the two CK1δ isoforms compared to the Δ400 truncation and the fully active, tail-less CK1δΔC. Activity was measured on a S665A mutant of the human PER2 FASP residues 645 to 687 fused to GST (Fig. 1*C* and *SI Appendix*, Fig. S1*C*). The S665A mutation only allows for phosphorylation of the rate-limiting priming serine at S662 (20). Although differences in activity were modest, the activity of CK1δ1 on the PER2 FASP was significantly lower than CK1δ2 (Fig. 1 *C* and *D*) and consistent with observed biological differences between CK1δ1 and CK1δ2 (26, 27). Truncation of the XCT or the entire tail also gave rise to activity that was similar to CK1δ2, recapitulating differences in the activity we observed in cells (27) and suggesting that CK1δ1 has increased autoinhibition. Tracking autophosphorylation with kinase assays (*SI Appendix*, Fig. S1 *C* and *D*) and Coomassie gel shift (*SI Appendix*, Fig. S1 *G* and *H*) showed that relative to the full-length proteins, the isolated kinase domain showed minimal autophosphorylation, and the δ1 kinase was significantly less phosphorylated than δ2 or Δ400, despite having more serines (*SI Appendix*, Fig. S1 *D* and *H*). These differences point to a potential regulatory role for the CK1δ1 XCT.

Regulation of XCT Autophosphorylation by Phosphatases in Cells. To test whether any of the XCT phosphorylation sites are indeed autophosphorylated in cells, we used an antibody that specifically recognizes a phosphorylated serine in the sequence SVV (pSVV antibody) that corresponds to S411 of CK1δ1 (*SI Appendix*, Fig. S1 *I* and *J*). This antibody detected robust autophosphorylation of purified full-length CK1δ1 (Fig. 1*E*). We then assessed phosphorylation of the XCT region in cells expressing myc-tagged CK1δ1. Phosphorylation of the CK1δ tail is regulated in vivo by an active cycle of autophosphorylation and dephosphorylation (7). Consistent with this, accumulation of S411 phosphorylation was only detected when cells were treated with calyculin A, a broad-spectrum inhibitor of cellular Ser/Thr phosphatases, revealing reversible phosphorylation of CK1δ1 S411 in cells (Fig. 1*F*). This is also consistent with reports of CK1δ1 phosphorylation at residues S406, S407, and S411 from large-scale phosphoproteomics screens (28, 29). Phosphorylation of CK1δ1 S411 in cells was blocked by addition of the CK1δ/ε-specific inhibitor PF6700462 (PF670) (Fig. 1*G*), indicating that it is primarily due to autophosphorylation. These data establish that S411 in the XCT of CK1δ1 is autophosphorylated in cells in a reversible and dynamic manner.

Our in vitro results clearly indicate that the length and phosphorylation status of CK1δ isoforms influence their kinase activity. Moreover, the finding of autophosphorylation and phosphatase-mediated dephosphorylation of the XCT region in cells demonstrates the potential for dynamic regulation of CK1δ1 activity in vivo. Multiple studies have reported regulation of CK1δ kinase activity from structural and biochemical perspectives, including examining the role of autophosphorylation of the tail region (12, 20–22, 26, 27, 30). These studies have not addressed how the recently described splice isoforms of CK1δ can regulate its kinase activity. Accordingly, we next employed NMR and HDX-MS to develop mechanistic insights into this process.

Differences in Regulation of the δ1 and δ2 Tails by the Kinase Domain. Possible phosphorylation sites in the tail have been mapped on full-length CK1δ1 in vitro (3) and in cells (31), where a nonphosphorylatable (NP) mutant substituting all 28 serines and threonines in the tail to alanine eliminated its electrophoretic mobility shift and regulation by cellular protein phosphatases (6). However, these studies did not unambiguously identify functionally important phosphorylation sites or regions required for autoinhibition. The δ1 tail is 125 amino acids long and predicted to be intrinsically disordered, and no part of it was captured in a crystal structure of the full-length kinase (32). Therefore, we turned to NMR spectroscopy to monitor backbone chemical shifts on the ^{15}N δ1 tail alone or in the presence of equimolar amounts of the unlabeled kinase domain to better understand potential regulatory mechanisms. The ^{15}N-^{1}H heteronuclear single quantum coherence (HSQC) spectrum of the isolated ^{15}N δ1 tail exhibited limited chemical shift dispersion consistent with an intrinsically disordered protein, and addition of the kinase domain in the absence of ATP resulted in very minor chemical shift perturbations (Fig. 2 *A*, *Left*), indicating that the tail and kinase domain did not interact in *trans* at these concentrations. However, incubation of the same sample with ATP for 2 h at 25 °C resulted in chemical shift perturbations in the ^{15}N δ1 tail backbone, as well as several new peaks downfield that correspond to phosphorylated residues (Fig. 2 *A*, *Right*), demonstrating that the kinase can phosphorylate its tail in *trans.*

Due to issues with peak overlap in the ^{15}N-^{1}H HSQC spectra, we turned to ^{13}C-direct detection experiments, using ^{15}N-^{13}C CON spectra that provide better resolution of the protein backbone in disordered proteins (33). Addition of unlabeled kinase to the ^{13}C,^{15}N δ1 tail in the absence of ATP showed minimal chemical shift perturbation in the tail, similar to our ^{15}N-^{1}H HSQC data (*SI Appendix*, Fig. S2*A*). After ATP addition, we observed chemical shift perturbations at the same resonances as in the HSQC (Fig. 2*B*), as well as some peak broadening upstream of XCT. Shifts were localized primarily to the XCT of the δ1 tail, and to a lesser extent in a charged region from residues 305 to 320

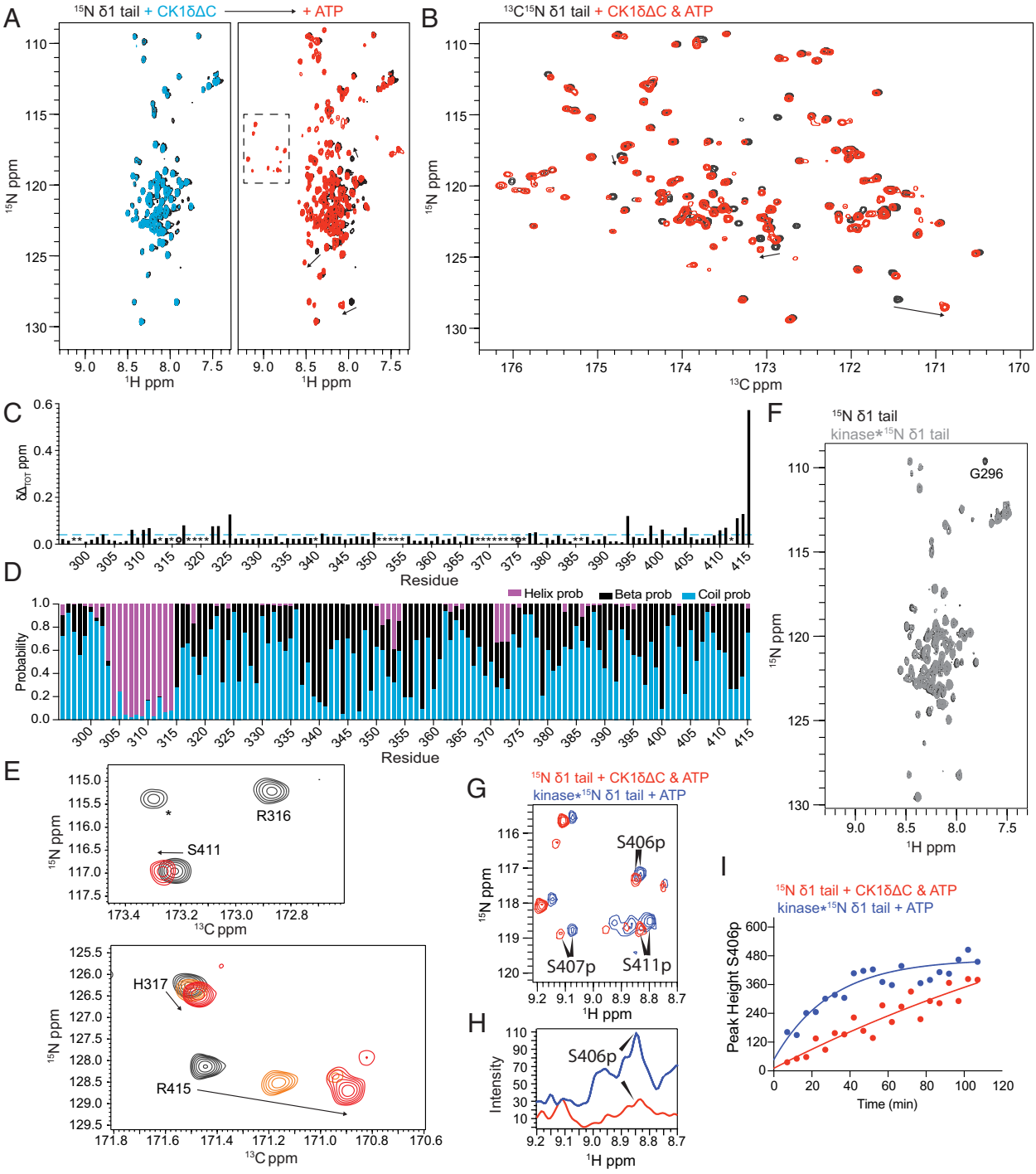

Fig. 2. Phosphorylation-dependent interaction of the δ1 tail with the kinase domain. (*A*) ^{15}N-^{1}H HSQC spectra of 100 μM ^{15}N δ1 tail alone (black) or in the presence of 100 μM CK1δΔC (blue) or 100 μM CK1δΔC and 2.5 mM ATP for 2 h at 25 °C (red); dashed box, peaks corresponding to phosphorylated residues. Arrows, chemical shift perturbation with phosphorylation. (*B*) ^{15}N-^{13}C CON spectra of 100 μM ^{13}C,^{15}N δ1 tail alone (black) or in the presence of 100 μM CK1δΔC and 2.5 mM ATP for 2 h at 25 °C (red). Arrows, chemical shift perturbation of the same peaks from panel *B*. (*C*) Quantification of chemical shift perturbations ($\Delta\delta_{TOT}$, ppm) from the ^{15}N-^{13}C CON spectrum of the δ1 tail alone or after incubation with CK1δΔC and ATP. Dashed line, significance cutoff at 0.05 ppm; open circle, broadened peaks; *, unassigned peaks. (*D*) Secondary Structure Propensity (SSP) analysis of the δ1 tail from chemical shift data. Random coil (blue), α-helix (pink), β-strand (black). (*E*) Zoomed in view of CON spectra showing phosphorylation-dependent changes in the extreme C terminus and predicted α-helical region. δ1 tail alone (black), with CK1δΔC and ATP for 2 h at 25 °C (red), or an unquenched partial phosphorylation reaction (orange). (*F*) ^{15}N-^{1}H HSQC spectra of 34 μM δ1 tail alone (black) or in segmentally labeled kinase (gray). G296, only residue broadened in full-length kinase. (*G*) ^{15}N-^{1}H HSQC spectra of ^{15}N δ1 tail with CK1δΔC and ATP in *trans* (red) or in *cis* (blue) with phosphopeak assignments. (*H*) ^{15}N-edited one-dimension (1D) ^{1}H spectra of phosphopeaks in panel *G*. (*I*) Quantification of 1D time course measuring phosphorylation of ^{15}N δ1 tail S406 in *trans* (red) or in *cis* (blue) with kinase.

that is predicted to have alpha-helical structure (Fig. 2 *C*–*E*). Peak broadening and chemical shift perturbations indicate that the XCT as well as some upstream residues are interacting with the kinase domain dependent on autophosphorylation. By contrast, ^{15}N-^{1}H HSQC spectra of the isolated δ2 tail showed chemical shift perturbations upon addition of the kinase domain alone (*SI Appendix*, Fig. S2 *B*, *Left*) that were enhanced by the addition of ATP (*SI Appendix*, Fig. S2 *B*, *Right*), suggesting that the δ2 tail interacts with the kinase domain in *trans* in a manner different from the δ1 tail. Peaks in the CON spectrum of the ^{13}C,^{15}N δ2

tail were significantly broadened compared to the δ1 tail (*SI Appendix*, Fig. S2 *C* and *D*), limiting further NMR analyses of the δ2 tail.

To determine how regulation of the δ1 tail is influenced when tethered to the kinase domain, we produced a segmentally isotopically labeled full-length kinase using an unlabeled kinase domain attached to an ^{15}N-labeled δ1 tail through Sortase A-mediated ligation (*SI Appendix*, Fig. S2*E*) (34, 35). ^{15}N-^{1}H HSQC spectra of the isolated ^{15}N-labeled δ1 tail and the tethered tail appeared to be the same, aside from broadening of a single glycine (G296) near the ligation juncture (Fig. 2*F*). Importantly, this suggests that the kinase domain and tail do not interact in the unphosphorylated state in *cis*. Addition of ATP to the tethered tail sample resulted in chemical shifts in the ^{15}N-labeled δ1 tethered tail backbone similar to those we observed in *trans* (compare Fig. 2*A* and *SI Appendix*, Fig. S2*F*), indicating that tethering did not substantially alter kinase domain interaction and phosphorylation of the tail, including activity on the XCT. To confirm this, we generated a minimal δ1 tail construct beginning at residue 376. We obtained chemical shift assignments for the phosphopeaks that correspond to the three phosphosites specific to the δ1 tail (Fig. 2*G*). Phosphorylation of these residues in the full-length CK1δ1 protein was confirmed by liquid chromatography (LC)/MS–MS (*SI Appendix*, Fig. S2*G*). Using ^{15}N-edited 1D ^{1}H spectra of the phosphoserine region (Fig. 2*H*), we were able to monitor the kinetics of phosphorylation of the δ1-specific residue S406. As expected, tethering increased the rate of phosphorylation compared to in *trans* (Fig. 2*I*) (36). Collectively, our NMR studies revealed differences in how the δ1 and δ2 tails interact with the kinase domain and demonstrated a preference for phosphorylation of the δ1-specific XCT serines by the kinase domain.

Impact of Phosphorylated FASP and CK1δ Tail on Structural Dynamics of the Kinase. Kinase domains interact with a number of ligands, from nucleotides and substrates to products and inhibitors, all of which can exert changes in dynamics or structure across the protein (37). To better understand autoinhibitory interactions between the kinase domain and tails of different CK1 isoforms, we turned to hydrogen–deuterium exchange mass spectrometry (HDX-MS) to characterize the conformational dynamics of different CK1δ isoforms. HDX-MS has been a powerful tool to provide insights into conformational dynamics in protein kinases (38–40). We first explored the effects of ATP or its nonhydrolyzable analogue AMPPNP binding on the isolated kinase domain using HDX-MS. Protection against deuterium incorporation upon binding to either nucleotide was predominantly observed across the N-terminal lobe and active site (*SI Appendix*, Fig. S3 *A* and *D*), with lower deuterium exchange in the bound state reflecting decreased solvent accessibility and increased H-bond formation between the nucleotide-interacting residues. At the active site, ATP binding led to stronger protection than AMPPNP (*SI Appendix*, Fig. S3*B*). These effects are similar to those observed for other kinases including PKA, ERK2, IRK, and SRC (41–44). In addition to these direct effects, the binding of ATP and AMPPNP also elicited distal conformational changes across the C-terminal lobe. Reduced deuterium exchange was observed across peptides spanning the DFG motif (residues 145 to 151), the activation loop (151 to 179), and loop L-EF (208 to 218), which are all centered around the substrate-binding cleft/groove (*SI Appendix*, Fig. S3*A*). No significant protection was detected in other regions of the C-lobe. Comparison of HDX-MS results also revealed other intrinsic dynamics of CK1δΔC, wherein peptides spanning the catalytic cleft and hinge region (residues 56 to 72) displayed bimodal isotopic distribution of mass spectra (*SI Appendix*, Fig. S3*C*). The two populations indicate the open and closed conformations of CK1δΔC that may be important for catalytic activity.

To validate HDX-MS as an approach to monitor inhibitory interactions on the kinase domain, we also looked at CK1δΔC in the presence of 4p-FASP, a phosphorylated inhibitory peptide from PER2 (20). Comparing HDX data of CK1δΔC in the absence and presence of 4p-FASP revealed a reduction in conformational flexibility throughout the kinase domain (Fig. 3*A*), with the largest effects observed at peptides covering the nucleotide-binding site (4–20), hinge region (56 to 72), activation loop (150 to 179), and substrate-binding cleft (residues 209 to 230) (Fig. 3*B*), close to two conserved anion-binding sites that mediate a direct interaction with the 4p-FASP peptide (20). Comparing the effects of 4p-FASP binding to the HDX profile of ATP-bound CK1δΔC (Fig. 3 *A* and *B*), we found that a larger segment of the activation loop and C-lobe had reduced solvent accessibility with 4p-FASP. These results illustrate how a phosphorylated product interacts with the substrate binding domain to substantially impact the conformational flexibility of CK1δ.

To explore how differences in isoform phosphorylation affect interactions within CK1δ, we preincubated CK1δΔC, CK1δΔ400, CK1δ1, and CK1δ2 for 15 min at 25 °C with excess AMPPNP or ATP to block or promote autophosphorylation, respectively, and then compared deuterium exchange profiles by HDX-MS (Fig. 3 *C–F*). The HDX-MS results, shown as Woods differential plots, highlight peptides that undergo significant protection from deuterium exchange in the presence of ATP in blue, while peptides with increased exchange are in red (Fig. 3 *C–F* and *SI Appendix*, Fig. S3 *E–H*). Similar to nucleotide alone, we observed protection in CK1δΔC in peptides covering primarily the N-lobe and substrate-binding groove (Fig. 3*C* and *SI Appendix*, Fig. S3*E*). Similar changes in HDX profiles were observed for CK1δΔ400, which lacks the XCT (Fig. 3*D* and *SI Appendix*, Fig. S3*F*). Two peptides at the junction between the kinase domain and the tail (residues 293 to 312 and 304 to 320) experienced a small but significant increase in deuterium exchange, indicating increased flexibility of this region upon ATP binding, although no other significant changes were observed along the C-terminal tail of CK1δΔ400 (Fig. 3*D* and *SI Appendix*, Fig. S3*F*).

The presence of CK1δ1 and CK1δ2 XCTs led to different degrees of protection upon autophosphorylation (Fig. 3 *E* and *F* and *SI Appendix*, Fig. S3 *G* and *H*). In the kinase domain, CK1δ2 differed from CK1δΔ400 by modestly enhancing protection of the nucleotide-binding pocket (Fig. 3*F* and *SI Appendix*, Fig. S3*H*). However, CK1δ1, with its preferential phosphorylation sites in the XCT, was strikingly different. CK1δ1 autophosphorylation led to a large majority of peptides (71 peptides in CK1δ1 versus only 32 in CK1δ2) showing significant protection spanning the N-lobe and the C-lobe. Peptides spanning the length of the disordered tail on CK1δ1 also showed significant protection, suggesting solvent inaccessibility, possibly due to interdomain interactions. CK1δ2 also had many peptides in the C-terminal tail that showed protection against deuterium exchange, albeit to a lesser extent (Fig. 3 *E* and *F* and *SI Appendix*, Fig. S3 *G* and *H*).

To further understand changes in structural dynamics mediated by phosphorylation, we analyzed residue-specific deuterium exchange by analysis of overlapping peptides, represented as heat maps for each construct (*SI Appendix*, Fig. S3*I*). These provide a comparative overview of time-dependent changes in exchange kinetics across the protein, including the C-terminal tail, and how truncation or splice isoforms influence this. These changes likely reflect both orthosteric effects of nucleotide-binding, as well as allosteric effects induced by the nucleotide and phosphorylation

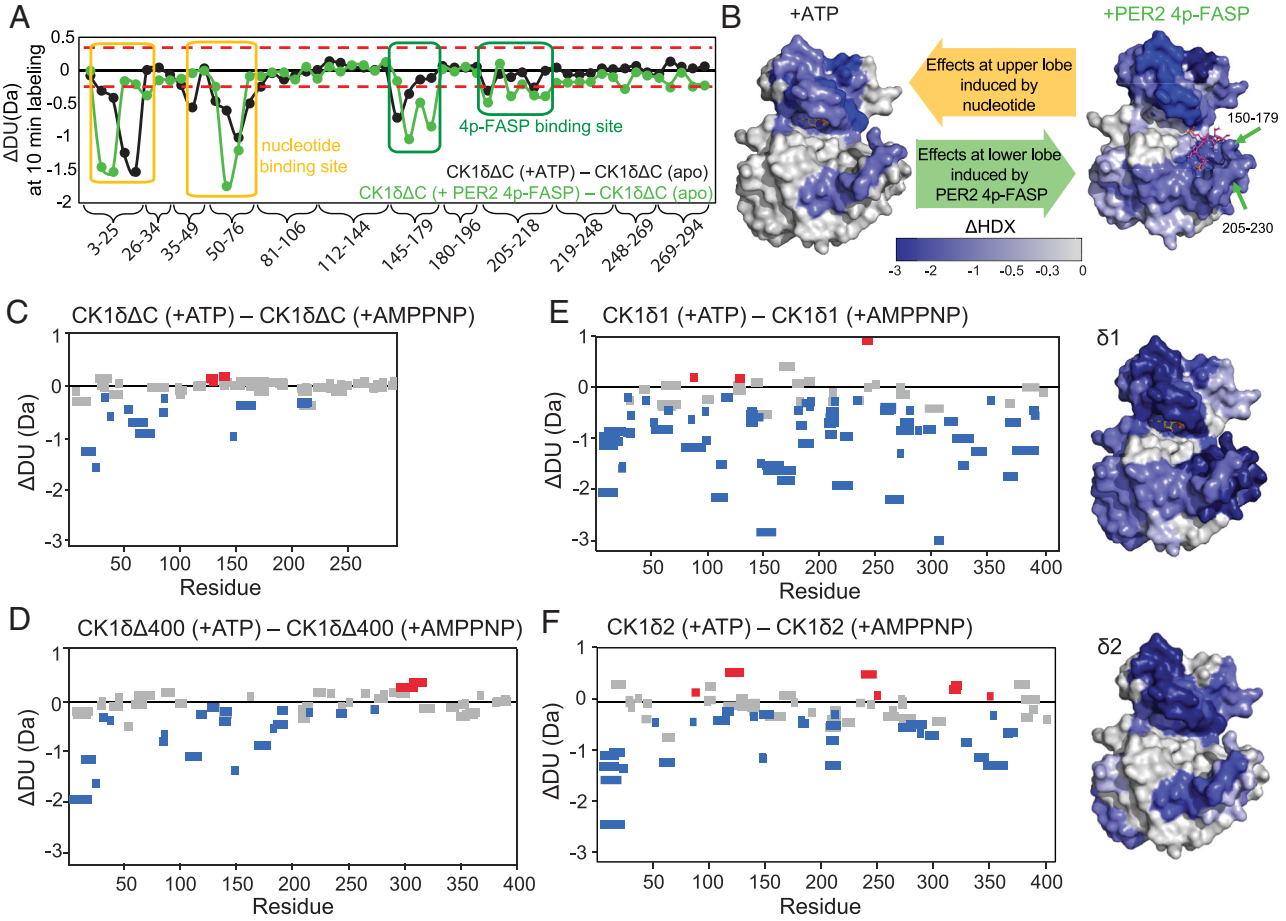

Fig. 3. Impact of phosphorylated FASP and CK1δ tail on structural dynamics of the kinase. (*A*) Comparison of differences in deuterium exchange of CK1δΔC in the presence and absence of 4p-FASP (green) or ATP (black) after 10 min labeling with residue numbers of the peptides grouped and indicated on the *x*-axis. Dashed line, significance threshold of ±0.28 Da. The deuterium exchange values are tabulated in *SI Appendix*, Table S1. (*B*) Structural representation of deuterium exchange at 10 min with ATP [*Left*, PDB: 6PXO, with ATP (yellow) from PDB: 6RU6] or 4p-FASP (*Right*, PDB: 8D7O). (*C–F*) Woods differential plots showing deuterium exchange between ATP-bound and AMPPNP-bound states of different CK1δ constructs: (*C*) CK1δΔC; (*D*) CK1δΔ400; (*E*) CK1δ1; and (*F*) CK1δ2 at 10 min labeling time. Data are available in *SI Appendix*, Table S2. Peptides showing significant protection (blue), deprotection (red), or nonsignificant (gray) deuterium exchange based on ±0.28 Da cutoff (CI 99.0%). (*E* and *F*) Corresponding structural representation of deuterium exchange differences at 10 min of CK1δ1 and CK1δ2.

of the C-terminal tail. Lower overall deuterium exchange across CK1δ2 suggests that the δ2 tail has different conformational dynamics and/or interactions with the kinase domain from the δ1 tail, consistent with our NMR data. Furthermore, the effect of different tail lengths on the conformational changes on the kinase domain is clear, with increases in deuterium exchange observed across most peptides of the kinase domain as the CK1δ1 XCT was removed (*SI Appendix*, Fig. S3 *J–M*).

Anion-Binding Sites on the Kinase Domain Play a Role in Autoinhibition by the δ1 Tail. One defining feature of CK1 is anion-binding sites near the active site that participate in substrate positioning and the conformation of the activation loop (22, 32). The phosphorylated PER2 pFASP peptide docks its phosphate groups into these sites that span the substrate binding cleft of the kinase, thus inhibiting kinase activity (Fig. 4 *A* and *C*) (20). We sought to determine whether the phosphorylated XCTs utilize these anion-binding sites to inhibit the kinase in a similar manner. First, we tracked changes in deuterium exchange of different kinase constructs in the presence and absence of ATP, looking specifically at several peptides that are proximal to anion-binding site 1 (Fig. 4*B*) and site 2 (Fig. 4*D*). For anion-binding site 1, CK1δ1 showed the greatest protection for all three peptides, with the 4pFASP-bound kinase, CK1δ2, and CK1δΔ400 showing moderate protection compared to CK1δΔC (Fig. 4*B*). For anion-binding site 2, CK1δ1 and the 4pFASP-bound kinase showed greater protection than the others (Fig. 4*D*).

To determine whether these sites play a role in inhibition by the tails, we looked at the effect of a single, well-characterized point mutation at each anion-binding site (22) on the ability of CK1δ1 or CK1δ2 to phosphorylate the PER2 FASP priming serine. Notably, these anion-binding site mutations eliminated inhibition by the phosphorylated PER2 FASP region (20). The K224D mutation impaired phosphorylation by CK1δ2 and CK1δΔC, which we attribute to impaired substrate positioning based on prior work (22). Remarkably, the same mutant in CK1δ1 had no decrease in FASP priming (Fig. 4*E* and *SI Appendix*, Fig. S4 *A* and *B*). Likewise, disruption of site 2 (R127E) had a similar isoform-specific effect on autoinhibition (Fig. 4*F* and *SI Appendix*, Fig. S4 *C* and *D*), although the effect was more modest than for site 1. We propose that the impaired substrate positioning caused by mutation of the anion-binding sites is counterbalanced by relief of autoinhibition in CK1δ1, perhaps due to reduced XCT binding at the mutated anion-binding sites.

To show the direct interaction of the phosphorylated XCT with the anion-binding sites, we generated a CK1δ1 construct with a minimal tail attached to the kinase domain that we called CK1δ-D1 tether (Fig. 4*G*). Kinase assays comparing CK1δ1, CK1δΔC, and CK1δ-D1 tether on PER2 FASP S665A show the tethered tail retains moderate inhibition (*SI Appendix*, Fig. S4 *E* and *F*). We then

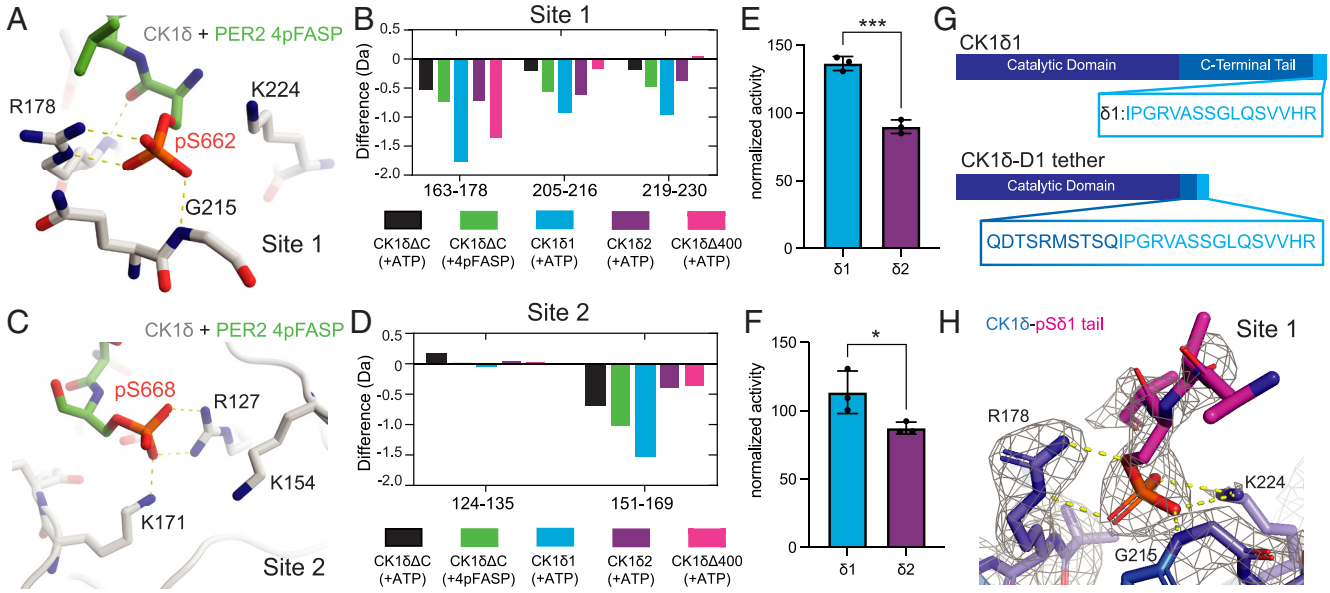

Fig. 4. Anion-binding sites on the kinase are required for autoinhibition by the δ1 tail. (*A*) Structural view of CK1δ bound to the inhibitory PER2 4p-FASP (PDB: 8D70) showing phosphate coordination by anion-binding site 1. (*B*) Comparison of protection from deuterium exchange of peptides spanning anion-binding site 1 with CK1δΔC (black), CK1δΔ400 (pink), CK1δ1 (blue), CK1δ2 (purple), and CK1δ-ΔC:4pFASP (green). (*C*) Structural view of CK1δ bound to the inhibitory PER2 4p-FASP (PDB: 8D70) showing phosphate coordination by anion-binding site 2. (*D*) Comparison of protection from deuterium exchange of peptides spanning anion-binding site 2. (*E* and *F*) ^{32}P kinase assays comparing the activity of K224D (*E*) or R127E (*F*) in CK1δ1 (blue) and CK1δ2 (purple) to WT, normalized to the effect of the mutant on the isolated kinase domain (*SI Appendix*, Fig. S5) (n = 3, mean ± SD). Significance was assessed by the unpaired two-tailed *t* test: **P* < 0.05; ****P* < 0.001. (*G*) Schematic of full-length CK1δ1 and CK1δ-D1 tether construct used for crystallization of the kinase with phosphorylated XCT. (*H*) 2Fo-Fc omit map of anion-binding site 1 (PDB: 9B3S) contoured at 1 σ highlighting residues on the kinase domain (blue), the phospho-tail (magenta), and polar contacts (yellow dashed lines).

solved a crystal structure of the autophosphorylated CK1δ-D1 tether, observing density for a phosphorylated serine docked into anion site 1. There was poor density for the sidechains of surrounding residues on the peptide, impeding the identification of the exact phosphor-serine(s) bound (Fig. 4*H*). This shows that the XCT directly interacts with anion site 1 in a similar manner to the inhibitory 4p-FASP (Fig. 4 *A* and *H*), demonstrating a conserved mechanism of inhibition.

Isoform-Specific Sequences of CK1δ Differentially Inhibit the Kinase Domain. Prior studies have shown that at least two substrates phosphorylated by CK1, the PER2 FASP region and the phosphorylation activation domain (PAD) of p63, inhibit kinase activity by-product inhibition (20, 21). To test whether this model holds for CK1δ tail autoinhibition, we added different phosphorylated δ1 or δ2 peptides to the kinase in *trans* (*SI Appendix*, Fig. S5*B*). To look at their effect on kinase activity, we used adenosine diphosphate (ADP)-Glo assays with two PER2 substrates, the FASP and the Degron, measuring activity with increasing phosphopeptide. For both substrates, inhibition by the δ1 peptides relied more on phosphorylation of the XCT, and the phosphorylated δ1 peptides were generally more potent inhibitors than the δ2 peptides, although there were some minor differences between the two substrates (Fig. 5*A* and *SI Appendix*, Fig. S5*A*).

We extended these findings to full-length CK1δ1 and tested whether the δ1-specific phosphosites are necessary for inhibition in the full-length protein in vitro. We mutated the three unique phosphosites in δ1 to alanines (S3A: S406A/S407A/S411A) and compared the activity to wild-type CK1δ1 on the PER2 FASP S665A substrate (Fig. 5*B* and *SI Appendix*, Fig. S5*C*). Consistent with the D1-A peptide data, the CK1δ1 S3A mutant showed a modest but significant increase in activity compared to CK1δ1 (Fig. 5 *B* and *C*), demonstrating that phosphorylation of the extreme C terminus is important for autoinhibition of CK1δ1. Coomassie gel shift assays also showed that CK1δ1 S3A shows a higher rate of autophosphorylation (Fig. 5*D* and *SI Appendix*, Fig. S5*D*), indicating the XCT also inhibits upstream autophosphorylation of other sites on the tail.

We next tested whether the S3A mutant altered the interaction and dynamics of the tail with the kinase domain as assessed by HDX-MS. Strikingly, we found a large decrease in protected peptides in CK1δ1 S3A relative to the wild-type enzyme (from 71 to 19, Fig. 5*E* and *SI Appendix*, Fig. S5*E*), spanning both the kinase domain and the C-terminal tail. The protection of the kinase domain by CK1δ1 S3A most closely resembled the HDX-MS behavior for CK1δΔC (Fig. 3*C*), suggesting a near-total loss of tail-kinase interaction in the mutant. Hence, phosphorylation of three serines in the CK1δ1 XCT is likely to be a prerequisite for the interaction of the C-terminal tail with the kinase domain.

These findings led us to examine how the CK1δ1 S3A mutation affected PER2 FASP phosphorylation and circadian rhythms in cells. Deletion of the C-terminal tail of CK1δ1 (CK1δΔC) or its S3A mutation markedly increased FASP priming site phosphorylation in full-length PER2 in cells (Fig. 5 *F* and *G*). To test how the S3A mutations influence circadian rhythms, we created PER2::LUC U2OS cell lines with stable overexpression of Flag-tagged CK1δ1 or the S3A mutant (*SI Appendix*, Fig. S5*F*). Expression of CK1δ1 S3A shortened the period by ~3 h relative to cells expressing CK1δ1 WT (Fig. 5 *H* and *I*), consistent with its overall increase in kinase activity. These results demonstrate that phosphorylation of the three CK1δ1-specific serines in the XCT is important for regulation of kinase activity in cells, where it contributes to period determination.

Discussion

CK1δ has been considered a constitutively active kinase because it does not require activation loop phosphorylation to take on an active conformation. Instead, it relies on autophosphorylation of its C-terminal tail and/or feedback inhibition from phosphorylation

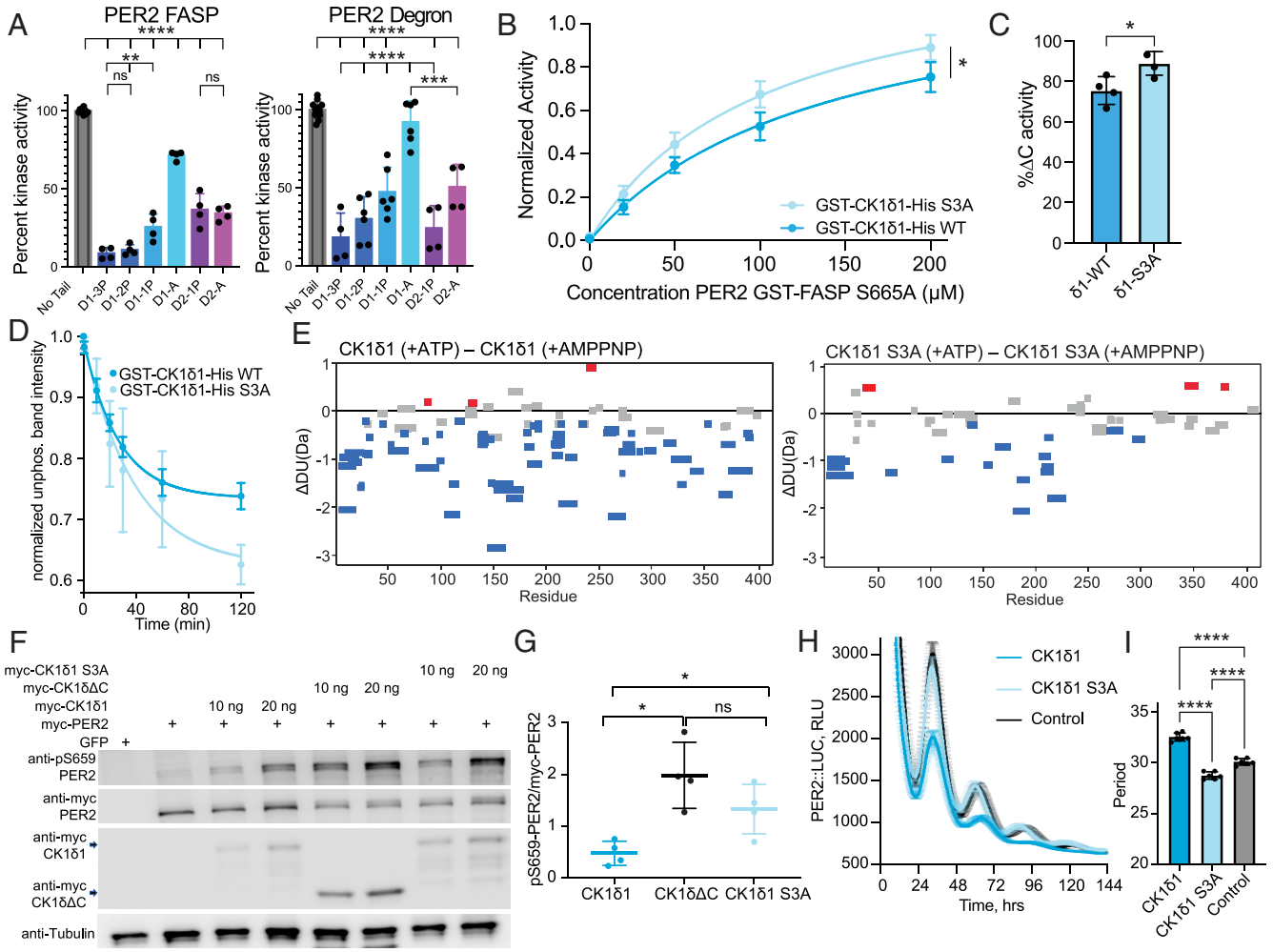

Fig. 5. Variable C-terminal tail length and mutations impact the kinase activity of CK1δ on its substrate PER2. (*A*) ADP-Glo kinase assay with phosphorylated CK1δ C-terminal peptides on PER2 FASP (*Left*) or Degron (*Right*). Significance was assessed by ordinary one-way ANOVA $^{**}P < 0.01$; $^{****}P < 0.0001$ (n = 2, mean ± SD). (*B*) ^{32}P kinase assay of CK1δ1 (blue) or the S3A mutant (light blue) on PER2 GST-FASP-S665A. Significance was assessed by the extra sum-of-squares F test (n = 3 mean ± SD). (*C*) Quantification of the endpoint (200 μM) in panel *C* (n = 3, mean ± SD). Significance was assessed by the unpaired two-tailed *t* test: $^{*}P < 0.05$. (*D*) Quantification of the unphosphorylated band intensity over time for CK1δ1 (blue) and CK1δ1 S3A (light blue) normalized to time 0 band intensity (n = 3, mean ± SD). (*E*) Woods differential plots showing deuterium exchange between ATP-bound and AMPPNP-bound states of CK1δ1 (*Top*) and CK1δ1 S3A (*Bottom*) at 10 min labeling. Data are available in *SI Appendix*, Table S2. Peptides showing significant protection (blue), deprotection (red), or nonsignificant (gray) deuterium exchange based on ±0.28 Da cutoff (CI 99.0%). (*F*) Representative western blot of mouse PER2 FASP priming phosphorylation (pS659) in HEK 293 lysates expressing indicated proteins (n = 4). (*G*) The ratio of pS659 to myc-PER2 was calculated and values are expressed in the *y*-axis. (n = 4 with mean ± SD). Significance was assessed by the unpaired two-tailed *t* test: $^{*}P < 0.05$. (*H*) Luminescence trace (shown in RLU) of PER2::LUC U2OS cells with stably expressed CK1δ1 (blue), CK1δ1 S3A (light blue), or no kinase control (black). (n = 6, ±SEM). Representative trace of n = 3. (*I*) Period analysis of panel *I* showing a lengthened period for CK1δ1 (blue) and a shortened period for CK1δ1 S3A (light blue) compared to control cells (black). Significance was assessed by ordinary one-way ANOVA, $^{****}P < 0.0001$. (n = 6, mean ± SD).

of its substrates to regulate kinase activity (3, 4, 20). While we are beginning to understand mechanisms of feedback inhibition (20, 21), the extent of intrinsic disorder and phosphorylation throughout the tail have impeded a mechanistic understanding of autoinhibition. Changes in circadian rhythms with two isoforms of CK1δ that differ only in the extreme C terminus of the tail demonstrate unambiguously that the tails have an important role in vivo (26, 27). However, it was not clear from these studies whether isoform-specific differences in activity were due to regulation of the tail by other kinases or whether they were intrinsic to CK1δ. Here, we show that CK1δ isoforms have inherent differences in activity arising from interactions of the kinase domain and its disordered tail that are specified by isoform-specific differences in autophosphorylation of the XCT. These differences explain the changes in period seen in the different CK1δ splice variants.

NMR spectroscopy allowed us to track site-specific autophosphorylation of the CK1δ disordered tails. We found that the three serines of the δ1-specific XCT are preferentially phosphorylated over other sites in the tail, whether the tail is phosphorylated by the kinase in *trans* or covalently linked to the kinase domain in *cis*. Chemical shift perturbations provided strong evidence for phosphorylation-independent effects of the kinase domain on the δ2 tail, although further analysis of the δ2 tail by NMR was limited due to extensive peak broadening in the absence of the kinase domain. This behavior is consistent with potential "fuzzy" intramolecular interactions within the δ2 tail, which may exhibit multiple transient conformations, as has been shown for other intrinsically disordered proteins (45, 46). Isoform-specific differences in the dynamics of the disordered tails could contribute to the decreased autoinhibition we observed with CK1δ2. Due to the sequence similarity of the XCT between CK1δ2 and CK1ε, the differences in tail dynamics we observed here could extend to CK1ε. Furthermore, the presence of disordered N- or C-terminal tails in CK1δ orthologs of other species also suggests that this could be a conserved mechanism of autoinhibition.

The phosphorylated PER2 FASP substrate inhibits CK1δ through interaction with conserved anion-binding sites that flank the substrate binding cleft to regulate circadian rhythms (20). HDX-MS analysis of the kinase domain bound to the inhibitory 4p-FASP phosphopeptide showed increased protection from deuterium exchange near these sites, confirming that our HDX-MS pipeline could map inhibitory interactions on the kinase domain. Of the two CK1δ isoforms, CK1δ1 showed the greatest deuterium protection across the kinase domain, including at sites protected by the 4p-FASP peptide. Protection in the kinase domain was moderately reduced in CK1δ2 and essentially eliminated by truncation of the XCT or the S3A mutant that eliminated phosphosites unique to δ1, indicating that phosphorylation of the XCT plays a crucial role in autoinhibition by CK1δ1. We also observed significant protection of the intrinsically disordered tail upon autophosphorylation of both CK1δ1 and CK1δ2 that was eliminated with truncation of the isoform-specific sequences. This suggests that both tails make extensive contact with the kinase domain, although we don't yet understand the specific details of these interactions. One recent study looked at autoinhibitory interactions of CK1δ1 in the context of kinase activity on p63, finding no requirement for any specific phosphorylation sites (47), while another demonstrated that different modes of autoinhibition by CK1δ and ε isoforms influence substrate specificity (30), perhaps by targeting different sites on the kinase. Although our crystal structure of the tethered δ1 XCT revealed a key role for site 1 in kinase binding, we were unable to resolve which phosphor-serine(s) of the δ1 XCT were bound.

Based on our results, we propose that autophosphorylation of the CK1δ tail in its XCT facilitates its interaction with the kinase domain to inhibit kinase activity. Here, we examined the effect of CK1δ autophosphorylation on PER2 substrates involved in a phosphoswitch that controls its stability and the period of circadian rhythms in mammals, including humans (12, 13). The phosphoswitch alone does not fully explain the difference in period displayed by overexpression of CK1δ1 WT and the S3A mutant; however, recent reports identified a role for CRY–PER–CK1δ complexes in phosphorylating the CLOCK subunit of the circadian transcription factor CLOCK:BMAL1 to suppress transcriptional activation of target genes by displacing the complex from DNA (15, 48, 49). Therefore, regulation of CK1δ activity by isoform-specific tails could have several roles in regulating circadian rhythmicity, not only through modulating the stability of PER2 but also by instigating transcriptional repression through promoting the release of CLOCK:BMAL1 from DNA. CK1 isoforms also have major roles in other pathways, such as apoptotic signaling (50, 51), Wnt signaling (52–54), and the cell cycle, where it is overexpressed in several cancers (55, 56). Interestingly, CK1 autophosphorylation is stabilized in a cell cycle-dependent manner (57), suggesting that understanding its regulatory mechanisms could begin to build a deeper understanding of this enigmatic kinase.

Resource Availability

Materials and Methods. Details on protein expression and purification; peptide synthesis; in vitro kinase assays; enzyme-linked immunosorbent assay; generation of cell lines; NMR analysis; and HDX-MS sample preparation and analysis can be found in *SI Appendix*.

γ*^{32}*P-ATP kinase assay. Reaction mixtures were prepared with 1 μM enzyme and 0 to 200 μM dilutions of the substrate as indicated at 25 °C. Reactions were initiated with the addition of 2 mM ATP containing 2 μCi of γ-32p ATP (Perkin Elmer). All reactions were quenched after an incubation time of 1 h. Sodium dodecyl sulfate polyacrylamide gel electrophoresis (SDS-PAGE) was performed on samples for each reaction, and the gels were dried before being transferred to a storage phosphor screen (Amersham Biosciences) overnight. Images were collected with Typhoon Trio (Amersham Biosciences), and data were analyzed by densitometry using Image J (NIH), Excel (Microsoft), and Prism (GraphPad).

Crystallization and structure determination. Crystallization was performed by the hanging-drop vapor-diffusion method at 22 °C by mixing an equal volume of protein with reservoir solution. The reservoir solution for CK1δ-D1 tether (5.5 mg/mL) was 0.21 mM succinic acid pH 5.5 and 17% (vol/vol) polyethylene glycol 3350. The crystals were looped and briefly soaked in a drop of cryopreservant reservoir solution with 20% (vol/vol) glycerol and then flash-frozen in liquid nitrogen for X-ray diffraction data collection. Datasets were collected at the 23-ID-D beamline at the Advanced Photon Source at the Argonne National Laboratory. Data were indexed, integrated, and merged using CCP4 software suite (58). Structures were determined by molecular replacement with Phaser MR (59) using anion-free CK1δΔC (PDB: 6PXO). Model building was performed with Coot (60) and structure refinement was performed with PHENIX (61). All structural models were generated using PyMOL Molecular Graphics System 2.5.4 (Schrödinger).

Western Blotting. Either purified protein samples or whole cell extracts of transfected HEK293 cells lysed with cell lysis buffer [50 mM Tris-HCl pH 8.0, 150 mM NaCl, 1% Nonidet P-40, and 0.5% deoxycholic acid containing Complete protease inhibitors (Roche) and PhosStop phosphatase inhibitors (Roche)] were analyzed by denaturing SDS-PAGE gel, which was transferred on polyvinylidene difluoride membrane (Immobilon, Millipore). Blot was further probed using indicated primary antibodies and appropriate secondary antibodies conjugated with HRP. Signal was detected with enhanced chemiluminescence reagents from Thermo Fisher Scientific. Densitometric analysis of western blot bands was performed using ImageJ software (NIH). The ratio of pS659 to myc-PER2 was calculated, and values are expressed in Fig. 5*G*.

NMR spectroscopy data acquisition. NMR spectra were collected on a Varian INOVA 600 MHz or a Bruker 800 MHz spectrometer equipped with a ^{1}H, ^{13}C, ^{15}N triple resonance z-axis pulsed-field-gradient cryoprobe. NMR kinase reactions were performed at 25 °C with 100 μM ^{13}C,^{15}N CK1δ1 tail or CK1δ2 tail, 2.5 mM ATP, and 100 μM CK1δ ΔC. Samples were incubated for 2 h and quenched with 20 mM ethylenediaminetetraacetic acid (EDTA), then ^{1}H-^{15}N HSQC spectra (total data acquisition = 20 min) and ^{13}C-^{15}N CON spectra (total acquisition time = 9 h 32 min) were collected. The incubation time to reach saturation of the kinase reaction with CK1δ1 short tail was determined by collecting a series of ^{1}H-^{15}N HSQC spectra (53 20-min spectra for a total acquisition time = 1,060 min) of 100 μM ^{13}C,^{15}N CK1δ1 short tail, 2.5 mM ATP, and 100 μM CK1δ ΔC at 25 °C. For phosphopeak assignments, the CK1δ1 short tail kinase reaction was then performed with 100 μM ^{13}C,^{15}N CK1δ1 short tail, 2.5 mM ATP, and 100 μM CK1δ ΔC incubated overnight at 25 °C and quenched with 20 mM EDTA; then, ^{1}H-^{15}N HSQC spectra (total data acquisition = 20 min), ^{13}C-^{15}N CON spectra (total acquisition time = 9 h 32 min), and triple-resonance experiments were collected.

Segmentally labeled NMR kinase reactions were performed at 25 °C with 34 μM CK1δ ΔC*-^{15}N CK1δ1 and 2.5 mM ATP. Samples were prepared as described above, and then ^{1}H-^{15}N HSQC spectra (total data acquisition = 2 h) were collected. For the phosphorylation kinetic assays, reactions were performed at 25 °C with 34 μM CK1δ ΔC*-^{15}N CK1δ1 tail, or 34 μM CK1δ ΔC* and 34 μM ^{15}N CK1δ1 tail in *trans*, and then, ^{15}N-edited 1D ^{1}H spectra were collected (224 data points at 6 min per spectrum for a total data acquisition = 1,344 min) immediately after the addition of 2.5 mM ATP. Spectra were processed using MestreNova (MestreLab), and data analysis was performed using Excel (Microsoft) and Prism (GraphPad).

Hydrogen–deuterium exchange mass spectrometry data acquisition. For nanoLC–MS/MS analyses, each quenched sample was subjected to in-line proteolysis using the Enzymate™ immobilized pepsin cartridge (Waters, USA). The digestion was left to proceed for 3 min at 12 °C, and the resulting peptide mixtures were analyzed with nanoACQUITY M-class UPLC (Waters, UK) equipped with a trapping column (VanGuard C18, 5 μm particle size) and an analytical column (ethylene bridged hybrid C18, 75 μm × 100 mm, 1.7 μm particle size) maintained at 3 °C to minimize back-exchange (62). The aqueous solvent was 0.1% formic acid in LC–MS grade water, and the organic solvent was 0.1% formic acid in HPLC-grade acetonitrile. A 10-min gradient was used to resolve and elute the peptides by reverse-phase chromatography. The peptides were then identified

by the Synapt G2-Si high-resolution mass spectrometer (Waters, UK). Briefly, the mass spectrometer was operated in positive polarity, data-independent fragmentation, and ion-mobility (high-definition mass spectrometry^{E}) mode separation. Mass spectrometer parameters were as described previously (63). Glu-fibrinopeptide reference (m/z = 785.8426) was continuously sprayed every 30 s during ESI-MS experiments using the lockspray device to ensure mass accuracy.

Materials availability. Plasmids generated in this study are available upon request.

Experimental Model and Subject Details.

Cell lines.

- The HEK293T cell line was purchased from ATCC (#CRL-3216).
- U2OS PER2::LUC cell line was a gift from John O'Neill (MRC LMB, UK).

Data, Materials, and Software Availability. NMR chemical shift assignments for the human CK1 δ1 tail; Coordinates for the CK1δ1-D1 tether structure data have been deposited in BMRB and PDB (52349 (64), 52375 (65), and 9B3S (66)). Some study data are available. Plasmids generated in this study are available upon request.

ACKNOWLEDGMENTS. Funding for this work was provided by the US NIH grants R01 GM107069 and R35 GM141849, and the HHMI (to C.L.P.) and Singapore Ministry of Health grant MOH-000600 to D.M.V. We thank Andrew D. Beale and John S. O'Neill (Medical Research Council Laboratory of Molecular Biology, UK) for their generous gift of the U2OS PER2::LUC cell line and Jae Kyoung Kim (Korea Advanced Institute of Science & Technology, Korea) for consultations on the mathematical model.

Author affiliations: [a]Department of Chemistry & Biochemistry, University of California Santa Cruz, Santa Cruz, CA 95064; [b]Department of Biological Sciences, National University of Singapore, Singapore 117543, Singapore; [c]Merck Sharp & Dohme International GmBH (Singapore), Neuros, Singapore 138665, Singapore; [d]Program in Cancer and Stem Cell Biology, Duke-National University of Singapore Medical School, Singapore 169857, Singapore; [e]Department of Pediatrics, Duke University Medical Center, Durham, NC 27710; [f]Center for Circadian Biology, University of California San Diego, La Jolla, CA 92093; and [g]HHMI, University of California, Santa Cruz, CA 95064

Author contributions: R.L.H., N.K.T., R.N., D.M.V., and C.L.P. designed research; R.L.H., N.K.T., R.N., N.Y., M.G.A.H., H.-W.L., P.C., and S.M.T. performed research; R.L.H., N.K.T., R.N., N.Y., M.G.A.H., and P.C. contributed new reagents/analytic tools; R.L.H., N.K.T., R.N., N.Y., H.-W.L., P.C., and S.M.T. analyzed data; D.M.V. and C.L.P. funding; and R.L.H., N.K.T., R.N., D.M.V., and C.L.P. wrote the paper.

1. M. Huse, J. Kuriyan, The conformational plasticity of protein kinases. *Cell* **109**, 275–282 (2002).
2. J. A. Endicott, M. E. Noble, L. N. Johnson, The structural basis for control of eukaryotic protein kinases. *Annu. Rev. Biochem.* **81**, 587–613 (2012).
3. P. R. Graves, P. J. Roach, Role of COOH-terminal phosphorylation in the regulation of casein kinase I delta. *J. Biol. Chem.* **270**, 21689–21694 (1995).
4. A. Cegielska, K. F. Gietzen, A. Rivers, D. M. Virshup, Autoinhibition of casein kinase I epsilon (CKI epsilon) is relieved by protein phosphatases and limited proteolysis. *J. Biol. Chem.* **273**, 1357–1364 (1998).
5. U. Knippschild *et al.*, The CK1 family: Contribution to cellular stress response and its role in carcinogenesis. *Front. Oncol.* **4**, 96 (2014).
6. G. W. L. Eng, D. M. Edison, Virshup, Site-specific phosphorylation of casein kinase 1 delta (CK1delta) regulates its activity towards the circadian regulator PER2. *PLoS One* **12**, e0177834 (2017).
7. A. Rivers, K. F. Gietzen, E. Vielhaber, D. M. Virshup, Regulation of casein kinase I epsilon and casein kinase I delta by an in vivo futile phosphorylation cycle. *J. Biol. Chem.* **273**, 15980–15984 (1998).
8. C. L. Partch, K. F. Shields, C. L. Thompson, C. P. Selby, A. Sancar, Posttranslational regulation of the mammalian circadian clock by cryptochrome and protein phosphatase 5. *Proc. Natl. Acad. Sci. U.S.A.* **103**, 10467–10472 (2006).
9. F. Liu, D. M. Virshup, A. C. Nairn, P. Greengard, Mechanism of regulation of casein kinase I activity by group I metabotropic glutamate receptors. *J. Biol. Chem.* **277**, 45393–45399 (2002).
10. J. P. Etchegaray *et al.*, Casein kinase 1 delta regulates the pace of the mammalian circadian clock. *Mol. Cell Biol.* **29**, 3853–3866 (2009).
11. H. Lee, R. Chen, Y. Lee, S. Yoo, C. Lee, Essential roles of CKIdelta and CKIepsilon in the mammalian circadian clock. *Proc. Natl. Acad. Sci. U.S.A.* **106**, 21359–21364 (2009).
12. R. Narasimamurthy, D. M. Virshup, The phosphorylation switch that regulates ticking of the circadian clock. *Mol. Cell* **81**, 1133–1146 (2021).
13. M. Zhou, J. K. Kim, G. W. Eng, D. B. Forger, D. M. Virshup, A Period2 phosphoswitch regulates and temperature compensates circadian period. *Mol. Cell* **60**, 77–88 (2015).
14. X. Cao, L. Wang, C. P. Selby, L. A. Lindsey-Boltz, A. Sancar, Analysis of mammalian circadian clock protein complexes over a circadian cycle. *J. Biol. Chem.* **299**, 102929 (2023).
15. R. P. Aryal *et al.*, Macromolecular assemblies of the mammalian circadian clock. *Mol. Cell* **67**, 770–782.e6 (2017).
16. Y. An *et al.*, Decoupling PER phosphorylation, stability and rhythmic expression from circadian clock function by abolishing PER-CK1 interaction. *Nat. Commun.* **13**, 3991 (2022).
17. J. C. Francisco, D. M. Virshup, Hierarchical and scaffolded phosphorylation of two degrons controls PER2 stability. *J. Biol. Chem.* **300**, 107391 (2024).
18. K. L. Toh *et al.*, An hPer2 phosphorylation site mutation in familial advanced sleep phase syndrome. *Science* **291**, 1040–1043 (2001).
19. Y. Xu *et al.*, Modeling of a human circadian mutation yields insights into clock regulation by PER2. *Cell* **128**, 59–70 (2007).
20. J. M. Philpott *et al.*, PERIOD phosphorylation leads to feedback inhibition of CK1 activity to control circadian period. *Mol. Cell* **83**, 1677–1692.e8 (2023).
21. J. Gebel *et al.*, p63 uses a switch-like mechanism to set the threshold for induction of apoptosis. *Nat. Chem. Biol.* **16**, 1078–1086 (2020).
22. J. M. Philpott *et al.*, Casein kinase 1 dynamics underlie substrate selectivity and the PER2 circadian phosphoswitch. *Elife* **9**, e52343 (2020).
23. P. L. Lowrey *et al.*, Positional syntenic cloning and functional characterization of the mammalian circadian mutation tau. *Science* **288**, 483–492 (2000).
24. M. R. Ralph, M. Menaker, A mutation of the circadian system in golden hamsters. *Science* **241**, 1225–1227 (1988).
25. Y. Xu *et al.*, Functional consequences of a CKIdelta mutation causing familial advanced sleep phase syndrome. *Nature* **434**, 640–644 (2005).
26. J. M. Fustin *et al.*, Two Ck1delta transcripts regulated by m6A methylation code for two antagonistic kinases in the control of the circadian clock. *Proc. Natl. Acad. Sci. U.S.A.* **115**, 5980–5985 (2018).
27. R. Narasimamurthy *et al.*, CK1delta/epsilon protein kinase primes the PER2 circadian phosphoswitch. *Proc. Natl. Acad. Sci. U.S.A.* **115**, 5986–5991 (2018).
28. F. Sacco *et al.*, Glucose-regulated and drug-perturbed phosphoproteome reveals molecular mechanisms controlling insulin secretion. *Nat. Commun.* **7**, 13250 (2016).
29. F. S. Oppermann *et al.*, Large-scale proteomics analysis of the human kinome. *Mol. Cell Proteomics* **8**, 1751–1764 (2009).
30. S. N. Cullati *et al.*, Substrate displacement of CK1 C-termini regulates kinase specificity. *Sci. Adv.* **10**, eadj5185 (2024).
31. P. V. Hornbeck *et al.*, PhosphoSitePlus, 2014: Mutations, PTMs and recalibrations. *Nucleic Acids Res.* **43**, D512–520 (2015).
32. K. L. Longenecker, P. J. Roach, T. D. Hurley, Crystallographic studies of casein kinase I delta toward a structural understanding of auto-inhibition. *Acta Crystallogr. D Biol. Crystallogr.* **54**, 473–475 (1998).
33. M. Bastidas, E. B. Gibbs, D. Sahu, S. A. Showalter, A primer for carbon-detected NMR applications to intrinsically disordered proteins in solution. *Concepts Magn. Reson.* **44**, 54–66 (2015).
34. Y. Kobashigawa, H. Kumeta, K. Ogura, F. Inagaki, Attachment of an NMR-invisible solubility enhancement tag using a sortase-mediated protein ligation method. *J. Biomol. NMR* **43**, 145–150 (2009).
35. C. S. Theile *et al.*, Site-specific N-terminal labeling of proteins using sortase-mediated reactions. *Nat. Protoc.* **8**, 1800–1807 (2013).
36. M. Dyla, M. Kjaergaard, Intrinsically disordered linkers control tethered kinases via effective concentration. *Proc. Natl. Acad. Sci. U.S.A.* **117**, 21413–21419 (2020).
37. K. Lorenzen, T. Pawson, HDX-MS takes centre stage at unravelling kinase dynamics. *Biochem. Soc. Trans.* **42**, 145–150 (2014).
38. L. Konermann, J. Pan, Y. H. Liu, Hydrogen exchange mass spectrometry for studying protein structure and dynamics. *Chem. Soc. Rev.* **40**, 1224–1234 (2011).
39. G. R. Masson *et al.*, Recommendations for performing, interpreting and reporting hydrogen deuterium exchange mass spectrometry (HDX-MS) experiments. *Nat. Methods* **16**, 595–602 (2019).
40. J. B. Sheetz, M. A. Lemmon, Y. Tsutsui, Dynamics of protein kinases and pseudokinases by HDX-MS. *Methods Enzymol.* **667**, 303–338 (2022).
41. S. R. Hubbard, Crystal structure of the activated insulin receptor tyrosine kinase in complex with peptide substrate and ATP analog. *EMBO J.* **16**, 5572–5581 (1997).
42. Y. Hamuro *et al.*, Phosphorylation driven motions in the COOH-terminal Src kinase, CSK, revealed through enhanced hydrogen-deuterium exchange and mass spectrometry (DXMS). *J. Mol. Biol.* **323**, 871–881 (2002).
43. T. Lee, A. N. Hoofnagle, K. A. Resing, N. G. Ahn, Hydrogen exchange solvent protection by an ATP analogue reveals conformational changes in ERK2 upon activation. *J. Mol. Biol.* **353**, 600–612 (2005).
44. Z. Shi, K. A. Resing, N. G. Ahn, Networks for the allosteric control of protein kinases. *Curr. Opin. Struct. Biol.* **16**, 686–692 (2006).
45. M. Arbesu, G. Iruela, H. Fuentes, J. M. C. Teixeira, M. Pons, Intramolecular fuzzy interactions involving intrinsically disordered domains. *Front. Mol. Biosci.* **5**, 39 (2018).
46. W. Wang, D. Wang, Extreme fuzziness: Direct interactions between two IDPs. *Biomolecules* **9**, 81 (2019).
47. M. Lambert *et al.*, Fuzzy interactions between the auto-phosphorylated C-terminus and the kinase domain of CK1delta inhibits activation of TAp63alpha. *Sci. Rep.* **13**, 16423 (2023).
48. X. Cao, Y. Yang, C. P. Selby, Z. Liu, A. Sancar, Molecular mechanism of the repressive phase of the mammalian circadian clock. *Proc. Natl. Acad. Sci. U.S.A.* **118**, e2021174118 (2021).
49. Y. Otobe *et al.*, Phosphorylation of DNA-binding domains of CLOCK-BMAL1 complex for PER-dependent inhibition in circadian clock of mammalian cells. *Proc. Natl. Acad. Sci. U.S.A.* **121**, e2316858121 (2024).
50. U. Knippschild *et al.*, The role of the casein kinase 1 (CK1) family in different signaling pathways linked to cancer development. *Onkologie* **28**, 508–514 (2005).
51. C. Brockschmidt *et al.*, Anti-apoptotic and growth-stimulatory functions of CK1 delta and epsilon in ductal adenocarcinoma of the pancreas are inhibited by IC261 in vitro and in vivo. *Gut* **57**, 799–806 (2008).
52. B. Del Valle-Perez, O. Arques, M. Vinyoles, A. G. de Herreros, M. Dunach, Coordinated action of CK1 isoforms in canonical Wnt signaling. *Mol. Cell Biol.* **31**, 2877–2888 (2011).
53. C. M. Cruciat, Casein kinase 1 and Wnt/beta-catenin signaling. *Curr. Opin. Cell Biol.* **31**, 46–55 (2014).

54. Z. H. Gao, J. M. Seeling, V. Hill, A. Yochum, D. M. Virshup, Casein kinase I phosphorylates and destabilizes the beta-catenin degradation complex. *Proc. Natl. Acad. Sci. U.S.A.* **99**, 1182–1187 (2002).
55. B. Schittek, T. Sinnberg, Biological functions of casein kinase 1 isoforms and putative roles in tumorigenesis. *Mol. Cancer* **13**, 231 (2014).
56. L. H. Rosenberg *et al.*, Therapeutic targeting of casein kinase 1delta in breast cancer. *Sci. Transl. Med.* **7**, 318ra202 (2015).
57. F. E. Serrano, D. A. Marzoll, B. Ruppert, A. C. R. Diernfellner, M. Brunner, CK1δ homeostasis by activity-dependent shuttling and degradation of orphan kinase. bioRxiv [Preprint] (2023). https://doi.org/10.1101/2023.02.13.528286 (Accessed 20 March 2024).
58. M. D. Winn *et al.*, Overview of the CCP4 suite and current developments. *Acta Crystallogr. D Biol. Crystallogr.* **67**, 235–242 (2011).
59. A. J. McCoy *et al.*, Phaser crystallographic software. *J. Appl. Crystallogr.* **40**, 658–674 (2007).
60. P. Emsley, B. Lohkamp, W. G. Scott, K. Cowtan, Features and development of Coot. *Acta Crystallogr. D Biol. Crystallogr.* **66**, 486–501 (2010).
61. P. D. Adams *et al.*, The Phenix software for automated determination of macromolecular structures. *Methods* **55**, 94–106 (2011).
62. T. E. Wales, K. E. Fadgen, G. C. Gerhardt, J. R. Engen, High-speed and high-resolution UPLC separation at zero degrees Celsius. *Anal Chem.* **80**, 6815–6820 (2008).
63. P. V. Raghuvamsi *et al.*, SARS-CoV-2 S protein:ACE2 interaction reveals novel allosteric targets. *Elife* **10**, e63646 (2021).
64. R. Harold, H.-W. Lee, C. Partch, Data from "Isoform-specific C-terminal phosphorylation drives autoinhibition of Casein Kinase 1." Biological Magnetic Resonance Data Bank. https://bmrb.io/data_library/summary/index.php?bmrbId=52349. Deposited 12 March 2024.
65. R. Harold, H.-W. Lee, C. Partch, Data from "Casein Kinase 1 delta 2 tail." Biological Magnetic Resonance Data Bank. https://bmrb.io/data_library/summary/index.php?bmrbId=52375. Deposited 27 March 2024.
66. R. Harold, N. Yaitanes, S. Tripathi, C. Partch, Data from "Crystal structure of casein kinase 1 delta 1 with tethered phosphorylated tail." Protein Data Bank. https://www.rcsb.org/structure/9b3s. Deposited 20 March 2024.